J Neurophysiol 118: 1092–1104, 2017.
First published May 24, 2017; doi:10.1152/jn.00240.2017.

RESEARCH ARTICLE | *Cellular and Molecular Properties of Neurons*

A balance of outward and linear inward ionic currents is required for generation of slow-wave oscillations

Jorge Golowasch,[1,2] Amitabha Bose,[2] Yinzheng Guan,[1] Dalia Salloum,[1] Andrea Roeser,[1,2] and Farzan Nadim[1,2]

[1]*Federated Department of Biological Sciences, New Jersey Institute of Technology and Rutgers University, Newark, New Jersey; and* [2]*Department of Mathematical Sciences, New Jersey Institute of Technology, Newark, New Jersey*

Submitted 30 March 2017; accepted in final form 19 May 2017

Golowasch J, Bose A, Guan Y, Salloum D, Roeser A, Nadim F. A balance of outward and linear inward ionic currents is required for generation of slow-wave oscillations. *J Neurophysiol* 118: 1092–1104, 2017. First published May 24, 2017; doi:10.1152/jn.00240.2017.—Regenerative inward currents help produce slow oscillations through a negative-slope conductance region of their current-voltage relationship that is well approximated by a linear negative conductance. We used dynamic-clamp injections of a linear current with such conductance, I_{NL}, to explore why some neurons can generate intrinsic slow oscillations whereas others cannot. We addressed this question in synaptically isolated neurons of the crab *Cancer borealis* after blocking action potentials. The pyloric network consists of a distinct pacemaker and follower neurons, all of which express the same complement of ionic currents. When the pyloric dilator (PD) neuron, a member of the pacemaker group, was injected with I_{NL} with dynamic clamp, it consistently produced slow oscillations. In contrast, all follower neurons failed to oscillate with I_{NL}. To understand these distinct behaviors, we compared outward current levels of PD with those of follower lateral pyloric (LP) and ventral pyloric (VD) neurons. We found that LP and VD neurons had significantly larger high-threshold potassium currents (I_{HTK}) than PD and LP had lower-transient potassium current (I_A). Reducing I_{HTK} pharmacologically enabled both LP and VD neurons to produce I_{NL}-induced oscillations, whereas modifying I_A levels did not affect I_{NL}-induced oscillations. Using phase-plane and bifurcation analysis of a simplified model cell, we demonstrate that large levels of I_{HTK} can block I_{NL}-induced oscillatory activity whereas generation of oscillations is almost independent of I_A levels. These results demonstrate the general importance of a balance between inward pacemaking currents and high-threshold K^+ current levels in determining slow oscillatory activity.

NEW & NOTEWORTHY Pacemaker neuron-generated rhythmic activity requires the activation of at least one inward and one outward current. We have previously shown that the inward current can be a linear current (with negative conductance). Using this simple mechanism, here we demonstrate that the inward current conductance must be in relative balance with the outward current conductances to generate oscillatory activity. Surprisingly, an excess of outward conductances completely precludes the possibility of achieving such a balance.

rhythmic activity; compensation; ionic currents; model; phase space

Address for reprint requests and other correspondence: J. Golowasch, Federated Dept. of Biological Sciences, NJIT, 100 Summit St., CKB 337, University Heights, NJ 07103 (e-mail: Golowasch@njit.edu).

LEAK CURRENTS are key determinants of neuronal excitability (Brickley et al. 2007; Lu and Feng 2012; Lutas et al. 2016; Rekling et al. 2000) and can be regulated by many different neuromodulators, which can modify the activity either to silence neurons or to induce spiking or oscillatory activity (Bayliss et al. 1992; Cymbalyuk et al. 2002; Egorov et al. 2002; Lu and Feng 2012; Lutas et al. 2016; Talley et al. 2000; van den Top et al. 2004; Vandermaelen and Aghajanian 1983; Xu et al. 2009). Leak currents have been proposed to control pacemaker rhythm generation (Amarillo et al. 2014; Blethyn et al. 2006; Cymbalyuk et al. 2002; Koizumi and Smith 2008; Lu and Feng 2012; Pang et al. 2009; Yamada-Hanff and Bean 2013; Zhao et al. 2010). Often, leak currents act to bring the membrane potential to within a range of voltage where other currents can activate and produce a new state of activity (Brickley et al. 2007; Lu and Feng 2012; Rekling et al. 2000; Yamada-Hanff and Bean 2013).

Regenerative inward currents, such as persistent Na^+ and low-threshold Ca^{2+} currents, are essential for the generation of oscillatory neuronal activity (Amarillo et al. 2014; Del Negro et al. 2002; Dunmyre et al. 2011; Jahnsen and Llinás 1984; McCormick and Huguenard 1992; Yamada-Hanff and Bean 2013; Zhao et al. 2010). These currents can be divided into two almost linear components, only one of which is sufficient and necessary to generate the oscillations (Bose et al. 2014; Zhao et al. 2010). Since this component is linear, we refer to it as a leak current; however, it has negative-slope conductance (hence, a negative-conductance leak current, I_{NL}). It is a leak current in the sense that, when combined with the standard leak current (I_L), the total current $I_{NL} + I_L$ remains linear, and yet it is a key determinant of neuronal excitability. The mechanism by which I_{NL} controls oscillatory activity is not simply by increasing or decreasing the leakiness (i.e., excitability) of the cell but by destabilizing the resting state of the cell (Bose et al. 2014), thereby increasing the voltage of the cell to a point at which outward currents can turn on and bring the voltage back to hyperpolarized levels. In this way, when I_{NL} dominates over I_L, the total linear current can be a de facto pacemaker current (Bose et al. 2014; Zhao et al. 2010).

Outward currents, primarily carried by K^+, play an essential role as currents that restore the polarization of the cells from which a new cycle of depolarization and hyperpolarization can emerge. Consequently, the kinetics of these currents are essen-

tial in determining the overall dynamics of the oscillatory activity (Bose et al. 2014). A balance between outward and inward currents is essential for the generation of oscillatory activity: too little K^+ current and the cell will be pushed toward, and sometimes locked in, a depolarized state; too much K^+ current and the increased leakiness will prevent it from escaping the hyperpolarized resting state. A growing number of recent studies indicate that ionic current levels may be linked via mechanisms involving ion channel coregulation (Bergquist et al. 2010; Linsdell and Moody 1994; MacLean et al. 2003). A consequence of this coregulation is that, in a population of neurons, various parameters of these different currents (most notably their amplitude or conductance) are correlated with one another (Amendola et al. 2012; Anderson et al. 2016; Anirudhan and Narayanan 2015; Goaillard et al. 2009; Golowasch 2015; Khorkova and Golowasch 2007; Roffman et al. 2012; Schulz et al. 2006, 2007; Srikanth and Narayanan 2015; Temporal et al. 2012, 2014). Such coregulation is likely to be involved in maintaining the balance of regenerative and outward ionic currents to regulate activity levels in oscillatory neurons.

In the stomatogastric nervous system, I_{NL}, corresponding to the negatively sloped portion of the modulator-activated inward current I_{MI} (Golowasch and Marder 1992b; Gray and Golowasch 2016; Swensen and Marder 2000), is a pacemaker current of the pyloric network pacemaker neurons (Bose et al. 2014; Zhao et al. 2010). This current underlies the slow oscillations observed in the presence of a variety of neuromodulators (Golowasch and Marder 1992b; Swensen and Marder 2000), even in the presence of the Na^+ channel blocker tetrodotoxin (TTX). Although I_{MI} is expressed by all pyloric neurons (Swensen and Marder 2000), when these neurons are synaptically isolated modulator-induced oscillations occur only in a small subset: the three electrically coupled neurons regarded as the pacemaker neurons of the network [2 pyloric dilator (PD) and 1 anterior burster (AB) neuron; Hooper and Marder 1987]. Why other pyloric neurons do not show pacemaker activity in the presence of modulators is unclear.

Using both theoretical and experimental methods, we test the hypothesis that the generation of slow-wave oscillations requires the correct balance of a linear pacemaker inward current and outward currents. Our hypothesis is based on the property that I_{NL} is sufficient to emulate the pacemaker I_{MI} (Bose et al. 2014). We show that this balance can only be produced in a subset of pyloric network neurons that express the appropriate levels of high-threshold K^+ currents. We further show how the induction of oscillatory activity depends on the interplay between the maximal conductance (g_{NL}) and equilibrium potential (E_{NL}) of I_{NL} and how these observations match our theoretical predictions.

METHODS

Experimental

Experiments were performed on identified neurons from the stomatogastric ganglion (STG) of male crabs (*Cancer borealis*). The animals were obtained at local markets in Newark, NJ and maintained in seawater tanks at 10–13°C. The entire stomatogastric nervous system, including the anterior commissural and esophageal ganglia, STG, and connecting and motor nerves, was dissected out as previously described (Selverston et al. 1976) and pinned down on a Sylgard-coated petri dish, and the STG was desheathed to allow for electrode impalement of the cell bodies. All preparations were continuously superfused with chilled (10–13°C) physiological *Cancer* saline (in mM): 11 KCl, 440 NaCl, 13 $CaCl_2$, 26 $MgCl_2$, 11.2 Trizma base, and 5.1 maleic acid, pH 7.4–7.5.

Extracellular recordings were performed with pin electrodes placed in petroleum jelly wells built around individual nerves and recorded differentially, relative to an electrode placed outside of the well, with an A-M Systems 1700 differential amplifier (A-M Systems, Carlsborg, WA). Intracellular recordings, current injections, and voltage clamp were performed with Axoclamp 2B amplifiers (Molecular Devices, Sunnydale, CA) with double impalements using 0.6 M K_2SO_4 + 20 mM KCl-filled borosilicate electrodes. Low-resistance electrodes (15–20 MΩ) were used for current injection and high-resistance electrodes (30–40 MΩ) for voltage measurement. Individual neurons were identified by matching intracellularly recorded action potentials to action potentials on identified motor nerves that innervate known muscles (Selverston et al. 1976).

In every preparation, action potentials were blocked by bath application of 10^{-7} M TTX (Biotium). This treatment effectively blocks all modulatory inputs, including peptidergic and cholinergic modulators that activate I_{MI} (Golowasch and Marder 1992b; Swensen and Marder 2000), therefore decentralizing the preparation.

The dynamic clamp technique was used to activate I_{NL} (Fig. 1*A*) or a cut-off version of I_{NL} that does not cross the current axis (Fig. 1*A*) and thus corresponds to a more realistic version of the negative-slope component of I_{MI} (Fig. 1*A*). A variety of values of I_{NL} parameters (Zhao et al. 2010) was tested. The dynamic clamp was implemented with NetClamp software (Gotham Scientific, http://gothamsci.com/NetClamp) on a 64-bit Windows 7 PC using a NI PCI-6070-E board (National Instruments).

Data acquisition was performed with a Digidata 1332A data acquisition board and pCLAMP 10.3 software (Molecular Devices). Injections of current in dynamic clamp were performed at 10 kHz and voltage recordings at 5 kHz. The following equations were used:

$$I_{NL} = g_{NL}[v - E_{NL}]$$

$$I_{NL-cut} = g_{NL}[v - E_{NL}]Heav(v - E_{NL})$$

For dynamic-clamp experiments involving the PD neuron, the values used for injection were 12 values of g_{NL} from −0.01 to −0.30 μS and the reference value of E_{NL} was set at 2 mV below the cell's resting potential (V_{rest}), typically resulting in E_{NL} = −67 to −58 mV. The value of E_{NL} was changed by increments of ±5 mV up to ±15 mV from this reference value (a total of 7 values). To detect oscillatory activity we used the criterion of a minimum of 5-mV trough-to-peak amplitude.

Ionic currents were measured in two-electrode voltage clamp. The high-threshold K^+ current (I_{HTK}) was measured with depolarizing voltage steps from a holding voltage of −40 mV to inactivate the transient K^+ current (I_A). I_A was measured with the same depolarizing voltage steps as for I_{HTK} but from a holding voltage of −80 mV and calculated by subtraction of I_{HTK} from these recordings (Zhao and Golowasch 2012).

Pharmacological agents were prepared immediately before use. Statistical analysis was performed with either SigmaPlot 12 (Systat) or Origin 8.5 (OriginLab) software.

Model

The equations that describe the full model involve currents for leak (I_L), negative-conductance leak with cutoff ($I_{NL\text{-}cut}$), and three potassium currents, delayed rectifier (I_{Kdr}), high-threshold (I_{HTK}), and an A current (I_A), are

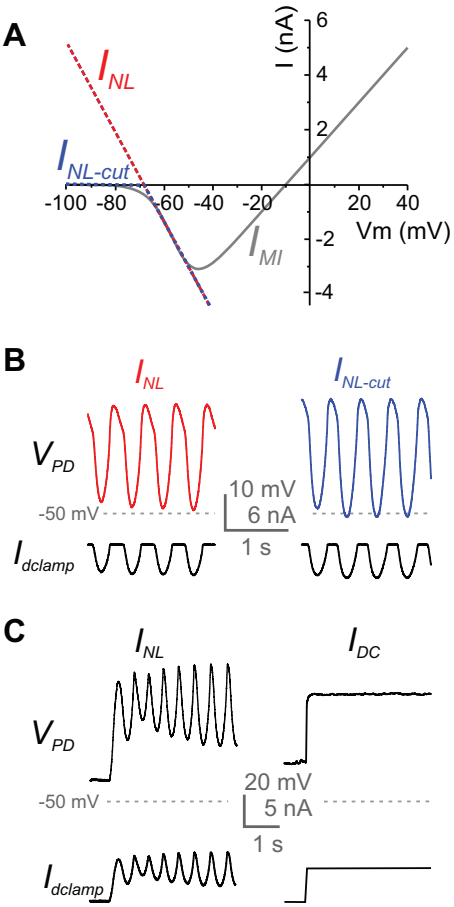

Fig. 1. Effect of I_{NL} injection in PD neurons. *A*: *I-V* curves of I_{MI} (gray), I_{NL} (red), and the truncated version of I_{NL} ($I_{NL\text{-cut}}$, blue). Note that both I_{NL} and $I_{NL\text{-cut}}$ are good approximations to the negatively sloped portion of I_{MI}, where $I_{MI} = g_{MI} m_\infty(v)[v - E_{MI}]$, $m_\infty(v) = \frac{1}{1+e^{-[v+10]/6}}$. *B*: effect of dynamic-clamp injection of I_{NL} (*left*) and $I_{NL\text{-cut}}$ (*right*) on the activity of PD neurons. Both traces are from the same neuron. *C*: injection of I_{NL} (*left*) and comparison with injection of constant current of the same time-averaged amplitude as I_{NL} (I_{DC}, *right*). Different preparation than in *B*. *Bottom* traces in *B* and *C* show the current injected by the dynamic clamp (I_{dclamp}).

$$C\frac{dv}{dt} = I_{ext} - g_L[v - E_L] - g_{NL}[v - E_{NL}]Heav(v - E_{NL})$$
$$- g_{Kdr} w[v - E_K] - g_{HTK} m_\infty(v)[v - E_K] - g_A wh[v - E_K]$$
$$\frac{dw}{dt} = \frac{w_\infty(v) - w}{\tau_K(v)}, \qquad (1)$$
$$\frac{dh}{dt} = \frac{h_\infty(v) - h}{\tau_A(v)}$$

The parameter C is the capacitance. The variable v represents the membrane potential, w is an activation variable for potassium currents that, for convenience, is taken to be common for both I_{Kdr} and I_A, and h is an inactivation variable for I_A. I_{HTK} is considered to have instantaneous activation and no inactivation. The parameters g_x and E_x represent the maximal conductance and reversal potentials for the various currents, respectively. We use the cutoff version $I_{NL\text{-cut}} = g_{NL}[v - E_{NL}]Heav(v - E_{NL})$ with a negative maximal conductance value g_{NL} (Fig. 1*A*). The Heaviside function $Heav(v - E_{NL})$ is 0 when $v < E_{NL}$ and is equal to 1 when $v \geq E_{NL}$. This implies that for $v \geq E_{NL}$, $I_{NL\text{-cut}}$ is simply a linear current with negative conductance, while for $v < E_{NL}$, $I_{NL\text{-cut}} = 0$ (Fig. 1*A*). The terms $w_\infty(v)$ and $m_\infty(v)$ are the steady-state activation functions for the two potassium currents, and $h_\infty(v)$ is the steady-state inactivation function of I_A. They are described by equations

$$w_\infty(v) = \frac{1}{1 + e^{-(v+40)/4}}, \quad m_\infty(v) = \frac{1}{1 + e^{-(v+25)/3}},$$
$$h_\infty(v) = \frac{1}{1 + e^{(v+50)/4}}$$

The associated time constants are given by

$$\tau_K(v) = \frac{3.9}{\cosh[(v + 40)/4]}, \quad \tau_A(v) = \frac{16.25}{\cosh[(v + 50)/4]}$$

Parameter values that vary across simulations are provided in RESULTS, while those that were fixed are given here: $C = 1\ \mu F/cm^2$, $g_L = 0.00325\ \mu S$, $E_L = -60$ mV, $g_{Kdr} = 0.0325\ \mu S$, $E_K = -80$ mV, and $I_{ext} = 0.065$ nA. These parameters were chosen so that the period of oscillations in the simulations was on the order of those found in experiments. Simulations and bifurcation diagrams were constructed with XPPAUT (Ermentrout 2002).

In prior work (Bose et al. 2014), we analyzed the case of $I_{HTK} = I_A = 0$ and showed that nonzero I_{NL} and I_{Kdr} currents alone can produce oscillations. To now isolate the effect of I_{HTK} with regard to pacemaker properties, for much of the analysis we continue to keep $I_A = 0$. With $I_A = 0$, the variable h is redundant and the set of equations in *Eq. 1* reduces to a two-dimensional system that is analyzed with phase-plane methods. We show that a nonzero value of I_A does not affect the existence of oscillations but that if it is large enough it can introduce a stable, subthreshold fixed point.

RESULTS

Pacemaker Current Operates Over Restricted Parameter Ranges

Our first goal here is to characterize some of the conditions that I_{MI} needs to satisfy to operate as a pacemaker current as predicted by our previous theoretical work (Bose et al. 2014). Oscillatory activity can be induced in the PD neuron by injecting the negative-leak conductance current I_{NL} (Fig. 1, *B* and *C*), which is a linearized version of the pacemaker current I_{MI} (Fig. 1*A*). The effect of I_{NL} only depends on the region of its current-voltage (*I-V*) curve where the current is negative. Therefore, injection of the same current that is set to 0 below E_{NL} (the cut-off version $I_{NL\text{-cut}}$) produces almost identical oscillations (Fig. 1*B*; see METHODS). Since the results for oscillatory activity are nearly identical, henceforth we use I_{NL}.

The effect of I_{NL} in producing oscillations in the PD neuron could not be mimicked by injecting a depolarizing DC current (Fig. 1*C*, *right*) equal to the time-averaged current measured during the dynamic-clamp injection of I_{NL} (Fig. 1*C*, *left*), demonstrating that the effects of I_{NL} are not simply a consequence of a depolarization of the cell by I_{NL} but its role as a voltage-dependent current.

In our previous study, we predicted that oscillations produced by I_{NL} would occur in a restricted range of g_{NL} (Bose et al. 2014). To explore the effect of the I_{NL} parameters on the oscillatory activity, we changed g_{NL} over 12 values from -0.01 to $-0.30\ \mu S$ and E_{NL} over a range of ± 15 mV in steps of ± 5 mV from the initial reference value (for a range of $12 \times 7 = 84$ runs; see METHODS). We found that there was a double Gaussian distribution ($R^2 = 0.9185$) of g_{NL}-E_{NL} values over which I_{NL} was effective in eliciting oscillatory activity (Fig. 2*A*).

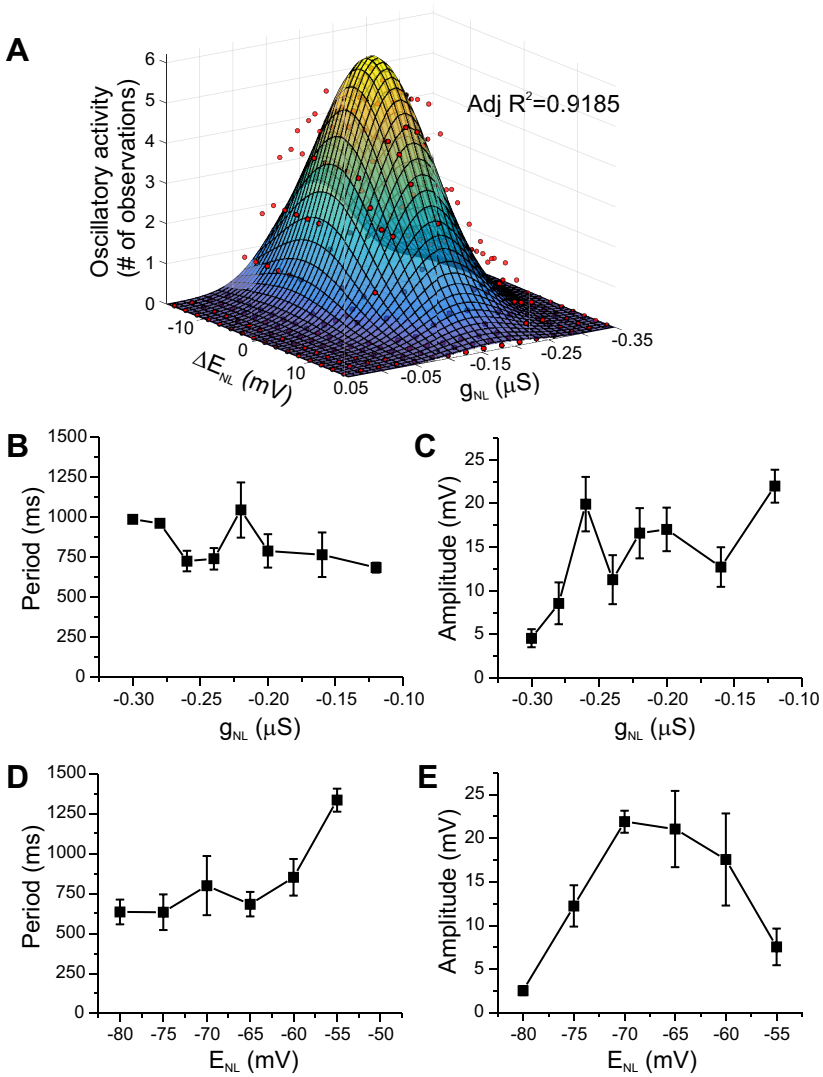

Fig. 2. Effect of I_{NL} parameters on PD neuron oscillations. Identified PD neurons (n = 7) were injected with dynamic-clamp I_{NL}, and parameters g_{NL} and E_{rev} were modified over a broad range of values. *A*: the presence or absence of oscillations (no. of oscillatory preparations out of 7) graphed as a function of the change in E_{rev} relative to each cell's resting voltage ($\Delta E_{NL} = 0 = V_{rest} - 2$ mV) and the value of the negative conductance injected (g_{NL}). Red symbols are the experimental data. The smooth surface is a Gaussian surface fit to the experimental data. Adjusted $R^2 = 0.9185$. *B*: mean period vs. g_{NL}. *C*: mean amplitude vs. g_{NL}. *D*: mean period vs. E_{NL}. *E*: mean amplitude vs. E_{NL}. All data shown in *A–E* are from the same set of cells. Error bars are SE.

An important point that these results illustrated was that oscillatory activity in the pyloric pacemaker cells does not require TTX-sensitive Na^+ currents to be produced. We observed a relative independence of cycle period on g_{NL} (Fig. 2*B*) but a decreasing amplitude of oscillations as g_{NL} became larger in absolute value (Fig. 2*C*). On the other hand, period was an increasing function of E_{NL} (Fig. 2*D*) and the oscillation amplitude had an inverted U-shape relationship with E_{NL} (Fig. 2*E*).

Pacemaker Cells Balance Inward and Outward Currents to Produce Oscillatory Activity

Effect of I_{HTK}. As we have seen, I_{NL} injected into neurons of the pacemaker group (i.e., PD neurons) consistently induces oscillatory activity (Fig. 2, Fig. 3, *top left*), albeit within relatively narrow ranges of g_{NL} and E_{NL} (Fig. 2). We examined whether follower neurons in the network were equally capable of generating oscillatory activity.

We observed that none of the follower cells in the pyloric network [ventral dilator (VD), pyloric constrictor (PY), inferior cardiac (IC), lateral pyloric (LP), and lateral posterior gastric (LPG) neurons] were capable of generating consistent oscillatory activity independently of the combination of g_{NL} and E_{NL} used. Individual examples shown in Fig. 3 were obtained by injection of $g_{NL} = -0.16$ μS and $E_{NL} = V_{rest} - 2$ mV for each cell type. However, each cell was further tested with the same combination of g_{NL} and ΔE_{NL} as the PD cells shown in Fig. 2*A*. We found that only one of eight LP neurons tested expressed any oscillatory activity, and none of the other follower cells tested could express such activity for any of the g_{NL} and E_{NL} combinations.

To understand what prevents follower cells from expressing oscillatory activity, we examined the levels of K^+ currents expressed in two of the follower cells (LP and VD neurons) and compared that to the current levels expressed by the pacemaker PD neurons. Our hypothesis throughout was that large outward currents could be responsible for preventing oscillatory activity. Figure 4 shows the comparison of two outward currents, I_{HTK} and I_A (see definitions in METHODS), with I_{HTK} further divided into peak (I_{HTK} peak) and steady state (I_{HTK} SS) in two cell types, the PD and LP neurons.

PD neurons expressed a significantly smaller I_{HTK} than LP neurons when this current was compared at its peak (2-way ANOVA, $P = 0.029$; Fig. 4*B*) as well as at steady state ($P < 0.001$; Fig. 4*C*). Interestingly, the activation parameters as well as the maximal conductance of the peak of I_{HTK} are not significantly different between PD and LP neurons (Fig. 4*E*;

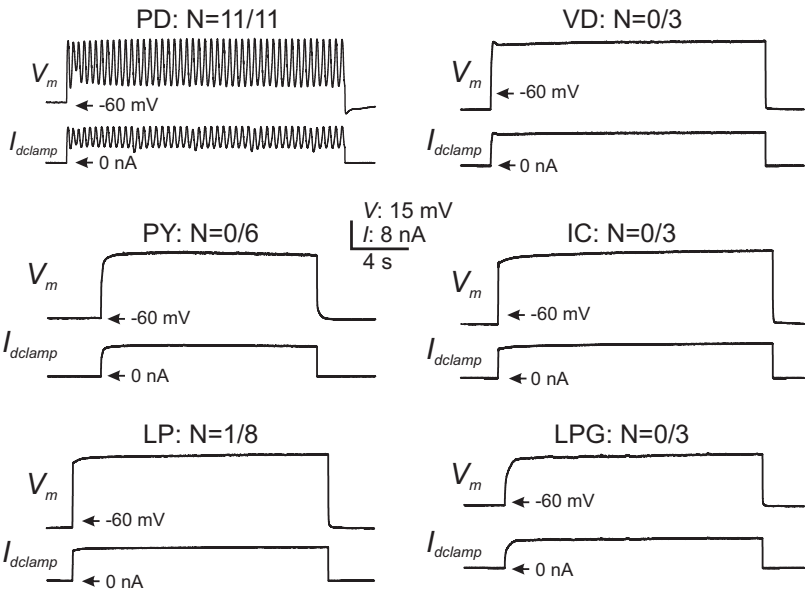

Fig. 3. Dynamic-clamp I_{NL} injection in pyloric network neurons cannot induce oscillatory activity in follower cells. Identified neurons with characteristic activity response to I_{NL} injection (g_{NL} = 0.16 μS, E_{NL} = V_{rest} – 2 mV) of the cells listed. PD neurons responded with oscillatory activity in 100% of the preparations tested. Numbers next to the cell type name indicate how many of the total cells tested showed any oscillatory activity. All cells were tested with the same combinations of g_{NL} and ΔE_{NL} as the PD neurons shown in Fig. 2*A*. *Top* trace in each panel is the membrane potential; *bottom* trace is the dynamic-clamp current injected.

PD, Table 1). However, the differences, especially in g_{max_HTK} and $V_{1/2\_HTK}$, while independently not significantly different between these cells, were sufficient to make the currents different between them.

In contrast to I_{HTK}, PD neurons had a significantly larger I_A than LP neurons (2-way ANOVA, P = 0.001, Fig. 4*D*) in part derived from a significantly more hyperpolarized activation curve ($V_{1/2\_A}$; Fig. 4*F*, Table 1) and a significantly higher maximum conductance (g_{max_A}; Table 1). The V_{slope} of I_A did not differ significantly between the two cells (Table 1).

Functional significance of K^+ current amplitude differences. To test whether the differences in K^+ current levels reported above are functionally related to the inability of follower cells to generate oscillatory activity when injected with I_{NL}, we reduced I_{HTK} with different concentrations of tetraethylammonium (TEA) (Golowasch and Marder 1992a) in the LP neuron.

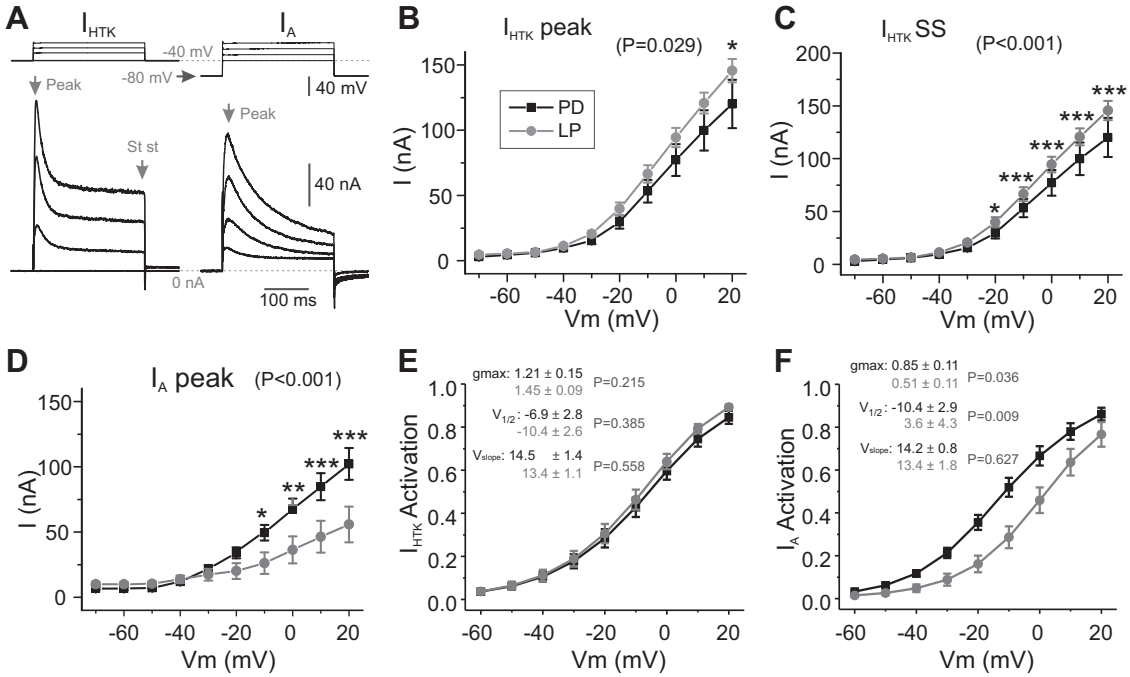

Fig. 4. Potassium current levels in 2 key pyloric network neurons. *A*: sample traces of I_{HTK} (*left*) and I_A (*right*). Vertical arrows point to the times at which I_{HTK} peak, I_{HTK} SS, and I_A are measured. *B*: *I-V* curves of the peak of the high-threshold current I_{HTK}. The curves are significantly different (2-way ANOVA, P < 0.029). *C*: steady-state *I-V* curves of I_{HTK}. The curves are significantly different (2-way ANOVA, P < 0.001). Asterisks indicate the source of the difference from 2-way ANOVA analysis and Tukey pairwise post hoc comparisons: *P < 0.05, **P < 0.01, *** P < 0.001. *D*: *I-V* curves of the peak of the transient K^+ current I_A. The curves are significantly different (2-way ANOVA, P < 0.001). Data in black for PD neurons and in gray for LP neurons. *E*: activation curves for I_{HTK} peak and the shown parameters are calculated as in *D*. *F*: mean of the voltage-dependent activation curves of I_A derived from the *I-V* curves of each cell used in *A*. The *I-V* curves were fit with the equation $I = g_{max}\frac{1}{1+e^{[V_{1/2}-v]/V_{slope}}}[v - E]$. *E* was fixed at −80 mV, and the other 3 parameters were determined from the fit ($V_{1/2}$ and V_{slope} in mV, g_{max} in μS). *P* values are for Student's *t*-test analysis for each parameter between the 2 cells. All error bars are SE.

Table 1. *I_{HTK} and I_A parameters in PD and LP neurons*

	Mean		SD			
	PD	LP	PD	LP	*t* (df)	*P*
g_{max_HTK}, μS	1.21	1.45	0.61	0.33	−1.270 (28)	0.215
$V_{1/2\_HTK}$, mV	−6.9	−10.4	11.6	9.3	0.883 (28)	0.385
V_{slope_HTK}, mV	14.5	13.4	5.8	3.8	0593 (28)	0.558
g_{max_A}, μS	0.85	0.51	0.44	0.39	2.205 (28)	0.036
$V_{1/2\_A}$, mV	−10.4	3.6	11.8	15.7	−2.829 (28)	0.009
V_{slope_A}, mV	14.2	13.5	3.4	6.5	0.491 (28)	0.627

Parameters were obtained from fits of a sigmoidal function to conductances calculated from I_{HTK} and I_A measurements and a driving force = ($V_m - E_{rev}$), with $E_{rev} = -80$ mV.

A significant effect of TEA on the I_{HTK} *I-V* curve is observed at all voltages [2-way repeated-measures (RM)-ANOVA, $P = 0.008$; Fig. 5*A*). In fact, a highly significant effect of TEA concentrations was observed, with a maximum inhibition level of ~80% and a half-maximal effect at 1.6 mM (Fig. 5*B*). We tested whether reduced I_{HTK} conditions were more permissive for producing oscillations by injecting I_{NL} ($g_{NL} = -0.16$ μS) in the presence of 8 mM TEA. We observed that, under these conditions, oscillatory activity could be consistently elicited in the LP neuron (Fig. 5*D*; $n = 4$) comparable to those generated by PD neurons (compare with Fig. 1*B*). As shown in Fig. 3, the same injection of I_{NL} in in the same cell under control conditions (0 mM TEA) could not trigger oscillatory activity in LP neurons (Fig. 5*C*).

Effect of I_A current amplitude differences. Because I_A also shows significantly different levels in the PD neuron compared with the LP neuron, albeit with higher levels in the PD neuron (Fig. 4*A*), we tested the effect of modifying I_A with the blocker 4-aminopyridine (4-AP) in PD neurons. We expected that, if I_A is involved in the regulation of PD neurons to generate oscillatory activity, reducing I_A levels in the PD neuron would affect its oscillatory properties. Figure 6 shows that 1 mM 4-AP significantly affects I_A overall (2-way ANOVA, $P = 0.012$ for 4-AP treatment), reducing it to levels similar to those measured in LP neurons, i.e., ~50% at all voltages tested (see Fig. 4*A*). Yet, application of 1 mM 4-AP had virtually no effect on the ability of these cells to oscillate in response to I_{NL} injection (compare Fig. 6*B* control with similar injection in the presence of 1 mM 4-AP in Fig. 6*C*).

Similar results were observed when comparing the PD and VD neurons, the latter another follower cell in the pyloric network. I_{HTK} in PD neurons was found to be significantly lower in amplitude across its voltage activation range than in VD neurons (2-way ANOVA, $P = 0.001$; Fig. 7*A*, Table 2), whereas, unlike the comparison of PD and LP neurons, there was no significant difference in I_A between these two cells (2-way ANOVA, $P = 0.787$; Fig. 7*B*).

Bath application of 8 mM TEA reduced the amplitude of I_{HTK} significantly (Fig. 7*C*; $n = 4$, 2-way RM-ANOVA, $P = 0.003$). The effect of TEA in the VD neuron was dose dependent (1-way RM-ANOVA, $P = 0.001$; Fig. 7*D*). When I_{NL} was injected ($g_{NL} = -0.08$ μS) in control medium (0 mM TEA), VD neurons such as the one shown in Fig. 7*E* depolarized but never generated oscillations (see also Fig. 3). However, in the presence of 8 mM TEA the same I_{NL} injection elicited oscillations (Fig. 7*F*) comparable to those produced by I_{NL} in PD neurons in normal TTX saline (Fig. 1, *B* and *C*) and LP neurons in TEA (Fig. 5*D*).

Modeling Description of Experimental Observations

We performed simulations using *Eq. 1* to determine whether a theoretical model provides a framework for understanding our experimental findings. The main question we investigated was whether differences in various K^+ currents could cause a model neuron to either oscillate or not. Additionally, we checked to see what computational predictions our model made with regard to period and amplitude as functions of parameters associated with I_{NL}.

To guide the simulations, we first discuss the phase-space structure of the model. Recall that we are keeping g_{Kdr} fixed throughout at 0.0325 μS and g_L at 0.00325 μS. This is to ensure oscillations in the absence of additional K^+ currents when I_{NL} is added. Now we examine the role of other K^+

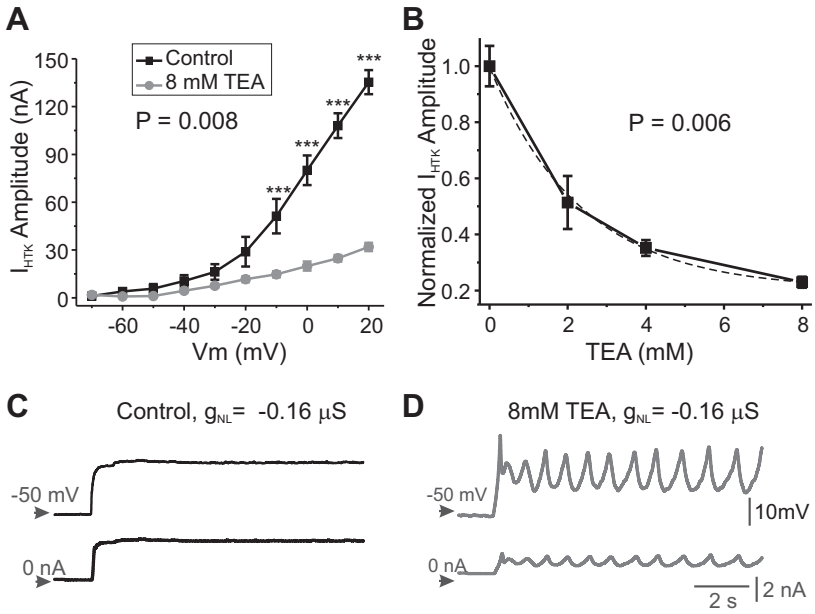

Fig. 5. High I_{HTK} levels are responsible for the inability of LP neurons to generate oscillatory activity. *A*: *I-V* curves of the peak I_{HTK} in LP neurons under control (0 mM TEA) and 8 mM TEA. A significant decrease is observed overall (2-way RM ANOVA, $n = 3$, $P = 0.008$), with asterisks indicating the source of the difference from Tukey pairwise comparisons: ***$P < 0.001$. *B*: dose-dependent sensitivity of peak I_{HTK} to TEA. I_{HTK} peak was normalized to the current measured in control (0 mM TEA). Mean ± SE is plotted. The overall effect was statistically significant (1-way RM ANOVA, $n = 3$, $P = 0.006$). Dashed trace is an exponential fit with a saturation level at ~20%, and an $ID_{50} = 1.6$ mM. *C*: effect of dynamic-clamp injection of I_{NL} ($g_{NL} = -0.16$ μS; $E_{NL} = -52$ mV) in control conditions. *Top*: membrane potential. *Bottom*: current injected by the dynamic-clamp circuit. *D*: effect of dynamic-clamp injection of I_{NL} (same as in *C*) but in the presence of 8 mM TEA.

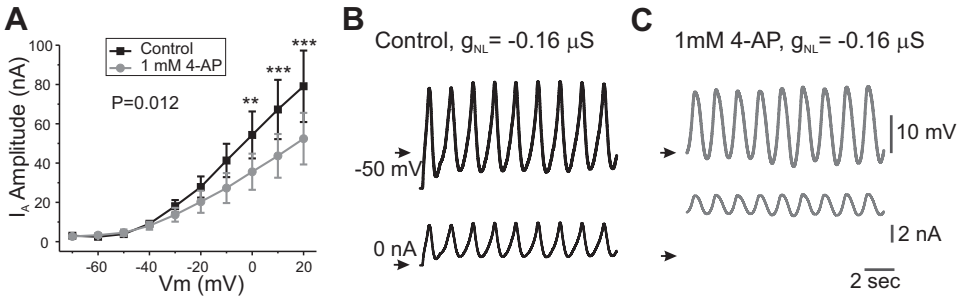

Fig. 6. I_A does not appear to be involved in the ability of PD neurons to generate oscillatory activity. *A*: *I-V* curves of the peak I_A in PD neurons under control (0 mM 4-AP) and 1 mM 4-AP. A significant decrease was observed overall (2-way RM-ANOVA, $n = 3$, $P = 0.012$), with asterisks indicating the source of the difference from Tukey pairwise comparisons: $^{**}P < 0.01$, $^{***}P < 0.001$. *B*: effect of dynamic-clamp injection of I_{NL} in the absence of 4-AP ($g_{NL} = -0.16$ μS; $E_{NL} = -72$ mV). *Top*: membrane potential. *Bottom*: dynamic-clamp current. *C*: effect of dynamic-clamp injection of I_{NL} in the presence of 1 mM 4-AP ($g_{NL} = -0.16$ μS; $E_{NL} = -72$ mV).

currents known to be expressed in most neurons, and in pyloric neurons in particular. When $I_A = 0$, the model equations involve only the v and w variables, allowing for phase-plane analysis. The nullclines of *Eq. 1* are obtained by plotting the set of points that satisfy $v' = 0$ and $w' = 0$, respectively. The v-nullcline is decreasing for $v < E_{NL}$. If $|g_{NL}|$ is sufficiently large relative to g_L, then the nullcline can increase for a range of values $v \geq E_{NL}$. The w-nullcline is a monotone increasing sigmoidal function. If it intersects the v-nullcline along its decreasing portion, then a stable fixed point ensues and oscillations are not possible. If the intersection of the two nullclines occurs for $v \geq E_{NL}$, then oscillations may be possible and

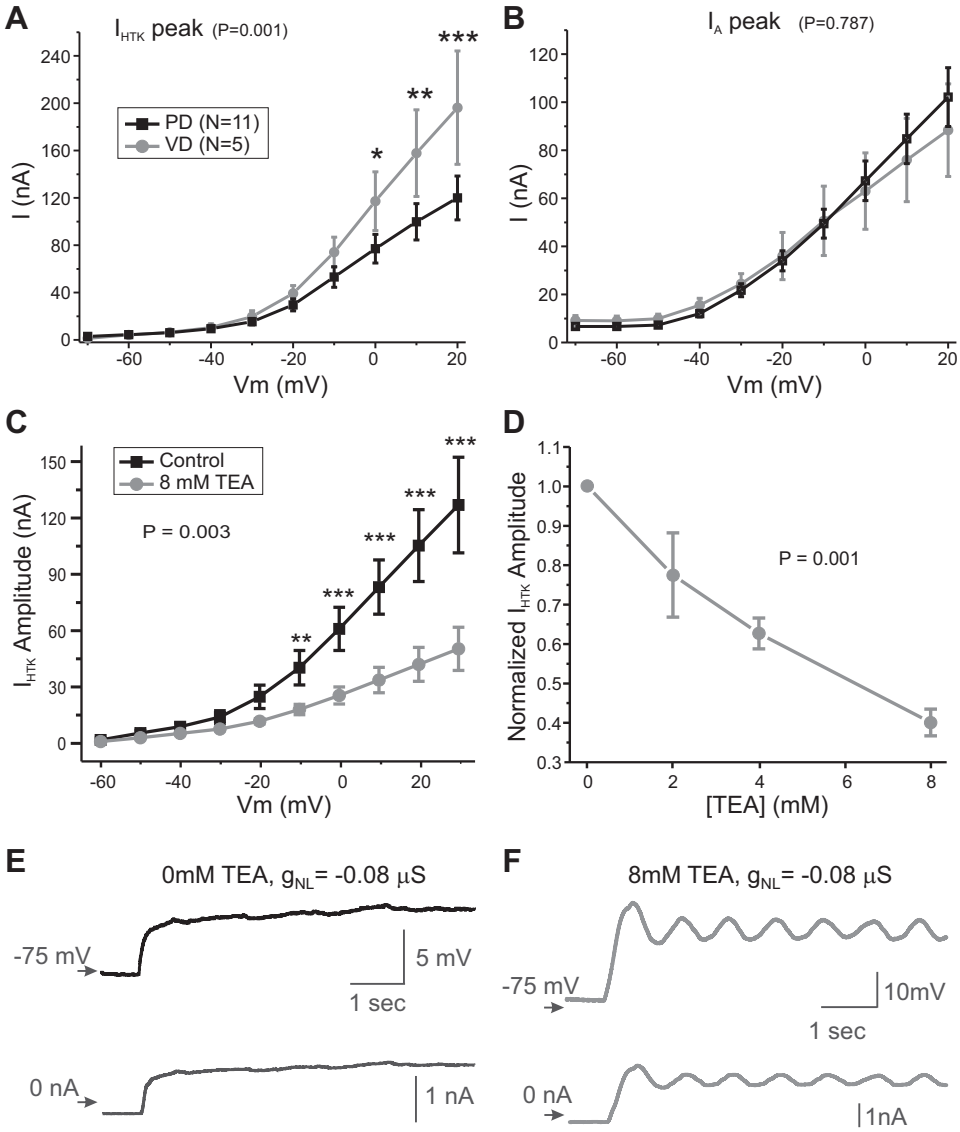

Fig. 7. High I_{HTK} levels are responsible for the inability of VD neurons to generate oscillatory activity. A: *I-V* curves show that the peak I_{HTK} in VD neurons is almost twice as large as in PD neurons (2-way ANOVA, $P = 0.001$) over most of its activation range. *B*: *I-V* curves of I_A show no significant difference between PD and VD neurons (2-way ANOVA, $P = 0.787$). *C*: *I-V* curves of the peak I_{HTK} in VD neurons under control (0 mM TEA) and 8 mM TEA. A significant decrease is observed overall (2-way RM ANOVA, $n = 4$, $P = 0.003$), with asterisks indicating the source of the difference from Tukey pairwise comparisons: $^{*}P < 0.05$, $^{**}P < 0.01$, $^{***}P < 0.001$. *D*: sensitivity of I_{HTK} peak of the VD neuron to TEA. I_{HTK} peak was normalized to the current measured in control (0 mM TEA). Mean ± SE is plotted. The overall reduction of I_{HTK} peak by TEA was significant (1-way RM ANOVA, $n = 4$, $P = 0.001$). *E* and *F*: effect of dynamic-clamp injection of I_{NL} ($g_{NL} = -0.08$ μS; $E_{NL} = -70$ mV) in normal saline (*E*) and in the presence of 8 mM TEA (*F*). *Top*: membrane potential. *Bottom*: current injected by the dynamic-clamp circuit.

Table 2. *I_{HTK} and I_A parameters in PD and VD neurons*

	Mean		SD			
	PD	VD	PD	VD	t (df)	P
g_{max_HTK}, μS	1.37	2.22	0.66	1.21	−1.894 (15)	0.078
$V_{1/2\_HTK}$, mV	−11.9	−13.5	9.8	13.5	0.274 (15)	0.788
V_{slope_HTK}, mV	16.8	14.9	6.1	6.0	0.605 (15)	0.554
g_{max_A}, μS	1.06	0.81	0.41	0.47	1.183 (15)	0.255
$V_{1/2\_A}$, mV	−12.5	−19.2	12.3	15.8	0.974 (15)	0.345
V_{slope_A}, mV	14.6	9.2	2.8	3.7	3.366 (15)	0.004

Parameters were obtained from fits of a sigmoidal function to conductances calculated from I_{HTK} and I_A measurements and a driving force = $(V_m - E_{rev})$, with $E_{rev} = -80$ mV.

depends on the slope of each at the point of intersection. We show that, as g_{HTK} is increased, oscillatory behavior is destroyed.

Figure 8*A1* shows the phase plane from *Eq. 1* when $g_{NL} = -0.0195$ μS, $g_{HTK} = 0.013$ μS, and $g_A = 0$ μS. For this choice of parameters, the *w*-nullcline intersects the *v*-nullcline along a portion where the latter is increasing with a sufficiently large slope at the point of intersection. This produces an unstable fixed point. A periodic solution surrounds this unstable fixed point because as *v* becomes too hyperpolarized I_{NL} current drives the voltage away from E_{NL}. At larger values of *v*, I_{Kdr} activates and restricts the voltage from increasing too much. This result is consistent with our prior work (Bose et al. 2014) in which I_{HTK} was not present. Thus the addition of this small amount of HTK conductance does not play a role in the generation of oscillations, but it does limit the amplitude at both higher and lower values of *v*. Indeed, the largest amplitude oscillation under these conditions exists when $g_{HTK} = 0$ (Fig. 8*B*).

We then increased the value of g_{HTK} to 0.0975 μS. Figure 8*A2* shows the ensuing phase plane. Note that the only change is that the *v*-nullcline now has a much steeper and pronounced right branch along which it is decreasing. Moreover, the slope of the *v*-nullcline at the intersection with the *w*-nullcline has decreased enough to stabilize that fixed point. This change is indicative of a Hopf bifurcation, which in fact occurs as g_{HTK} is increased. Figure 8*B* shows that as g_{HTK} is increased from lower values the periodic solution decreases in amplitude (upper and lower bounds of oscillations shown by solid gray curves); moreover, the unstable fixed point (dashed curve) gains stability through a Hopf bifurcation near $g_{HTK} = 0.078$ μS, and oscillations cease to exist. The reason for this loss of excitability is that I_{HTK} is too strong and destroys the balance between I_{Kdr} and $I_{NL\text{-}cut}$ that could produce oscillations. In short, too much I_{HTK} is incompatible with the production of oscillations. This finding is consistent with our experimental results shown in Figs. 5 and 6.

We next varied g_{NL} to further understand the relationship between these currents. Figure 8*C* shows bifurcation diagrams for three different fixed values of g_{HTK}, indicated by arrows from Fig. 8*B*, as we vary g_{NL}. Figure 8*C3* shows that if g_{HTK} is too large then no amount of $I_{NL\text{-}cut}$ can produce oscillations. Indeed for all values of g_{NL}, the stable fixed point remains. For smaller values of g_{HTK} (Fig. 8, *C1* and *C2*), oscillations are present over an interval of g_{NL} values (voltage traces shown in Fig. 8, *D1* and *D2*, respectively). This interval is a decreasing function of g_{HTK} as summarized in Fig. 8*E*. There, we show a two-parameter bifurcation diagram where the curve is the boundary between oscillatory and nonoscillatory behavior. For any choice of parameters that lies within the gray shaded parabola-like region, oscillations are possible. For choices outside of this region, oscillations are not possible. The diagram clearly shows that the interval of g_{NL} values over which oscillations occurs shrinks as g_{HTK} is increased.

Our experimental findings, as summarized in Fig. 7, suggest that I_A plays no role in generating oscillations but may affect the properties of the oscillatory solution. Therefore, we investigated what role, if any, I_A may play in the generation of oscillations. With a non-zero value of I_A, *Eq. 1* becomes three-dimensional and direct phase-plane analysis is not possible. Thus we now project the solution trajectory onto the *v*-*w* phase plane to study how the shape of the respective nullclines varies as a function of parameters associated with I_A. For example, Fig. 9*A1* shows the case where $g_A = 0.0325$ μS. Note that the projected nullclines look very much the same as those in Fig. 8*A1*. As we varied the value of either g_A or the half-activation voltage of $h_\infty(v)$, we found little change in the shape of the projected nullclines. Thus we concluded that the addition of I_A plays no role in whether a periodic solution exists, consistent with results of the prior subsection. However, an interesting effect of a large I_A current was found to occur. A very strong *A* current can induce bistability between a periodic solution and a stable fixed point. Figure 9*A2* shows the case of $g_A = 0.195$ μS. For this parameter value, a stable periodic solution coexists with a stable fixed point. The figure shows an example of a trajectory that starts at the stable fixed point where $h = 0.45$ (lower *v*-nullcline). Leaving the initial values of *v* and *w* unchanged, we switched to the initial condition $h = 0$. This has the effect of assigning a new initial condition in the full three-dimensional *v*-*w*-*h* phase space that is not a fixed point (though the location looks unchanged in the projection onto the *v*-*w* phase plane). The ensuing trajectory leaves that location and is seen to converge to the stable periodic orbit. The associated bifurcation diagram in Fig. 9*B* shows that the stable fixed point loses stability through a subcritical Hopf bifurcation as g_A is decreased. The gray roughly horizontal curves depict the upper and lower limits of the periodic solution.

Note that the bifurcation diagram is also a projection onto the *v*-g_A space. In this projection, the value of *h* for the fixed point cannot be discerned. Indeed, the bifurcation diagram at $g_A = 0.195$ μS suggests that the stable periodic solution encloses the stable fixed point (Fig. 9*B*). But from the projected phase plane in Fig. 9*A2* it appears that the stable periodic solution encloses an unstable fixed point. In reality, neither case is true. There is a stable fixed point whose projection in the *v*-*w* phase plane occurs at the intersection of the lower *v*-nullcline and the *w*-nullcline in Fig. 9*A2*, and which occurs for $h = 0.45$. The intersection of the upper *v*-nullcline and the *w*-nullcline is not a fixed point, as the value of *h* is not constant along the periodic solution. Instead, it is oscillating near $h = 0$. In addition, the periodic solution has lower and upper *v* limits that are smaller and larger than the *v* value at the stable fixed point. This is why the bifurcation diagram misleadingly suggests that the stable periodic solution encloses the stable fixed point.

Figure 10 shows model predictions for how the period and amplitude of oscillations depend on either g_{NL} (Fig. 10, *A* and

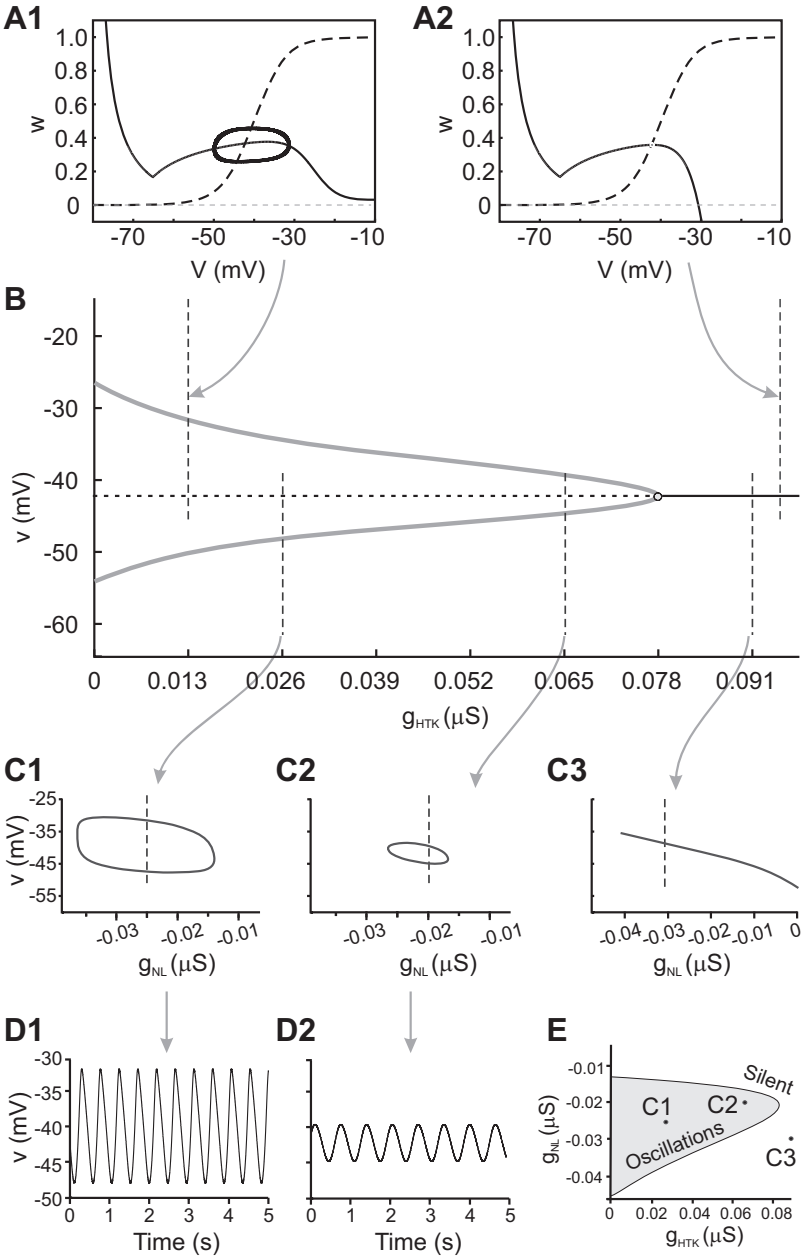

Fig. 8. Effect of I_{HTK} on the existence of oscillations. *A*: *A1* shows the *v*-*w* phase plane for low values of g_{HTK} in which an oscillatory solution exists (shown as dark closed path). For larger values of g_{HTK} the oscillatory solution fails to exist, as shown in *A2*, because the stronger I_{HTK} stabilizes the fixed point at the intersection of the 2 nullclines. *B*: bifurcation diagram showing how the existence and amplitude of oscillatory solutions depend on g_{HTK}. Gray curve indicates the voltage limits of oscillatory solutions, whereas the black line indicates a fixed point. Solid and dashed lines indicate stable and unstable fixed points, respectively. Arrows from *A1* and *A2* show the values of g_{HTK} used to produce those simulations. Oscillatory solutions are lost through a Hopf bifurcation as g_{HTK} increases. *C*: bifurcation diagrams showing behavior of solutions at fixed values of g_{HTK} while g_{NL} is varied. The range of g_{NL} values for which oscillations exist decreases as g_{HTK} increases (compare *C1* and *C2*). If g_{HTK} is too large (*C3*), no amount of g_{NL} can restore oscillations. *D1* and *D2*: voltage traces corresponding to the dashed lines in *C1* and *C2*, respectively. *E*: behavior of the model in the g_{HTK}-g_{NL} parameter space. Oscillations are limited to parameter values in the gray region.

B) or E_{NL} (Fig. 10, *C* and *D*). In all cases, the model is consistent with experiments in that the oscillations exist over a bounded interval of both g_{NL} and E_{NL}. Over a range of parameters, the model also qualitatively reproduces the dependence of period on both g_{NL} and E_{NL} (compare Fig. 10*A* to Fig. 2*B* and Fig. 10*C* to Fig. 2*D*).

The dependence of the amplitude of oscillations on g_{NL} and E_{NL} (Fig. 10, *B2* and *D2*, respectively) is obtained by subtracting the upper value of voltage from the lower value (upper branch of grey curve minus lower branch of gray curve) in Fig. 10, *B1* and *D1*. The model does a poor job of describing the larger-amplitude oscillations that arise in experiments for small absolute values of g_{NL} (compare Fig. 10*B2* with Fig. 2*C*). Mathematically this is because oscillations in the model arise because of a supercritical Hopf bifurcation, whereas those that arise in the experiments may correspond to a subcritical Hopf bifurcation. The dependence of amplitude on E_{NL} (compare Fig. 10*D2* with Fig. 2*E*) is reasonably well described qualitatively by the model. Oscillations begin at small amplitude at low values of E_{NL} due to a supercritical Hopf bifurcation. There is a local maximum in the amplitude at higher values of E_{NL}, followed by a decrease in the amplitude just before oscillations cease to exist.

In sum, the simulations provide a theoretical framework to support the notion that the balance between high-threshold outward currents and I_{NL} is critical to create preconditions for the existence of oscillations. Once this is in place, the simulations confirm that too much I_{HTK} (or too little total outward current) destroys this balance and thus can be used to determine which pyloric neurons can actually produce oscillations based on the I_{NL} protocol. The model also confirms that I_A does not appear to play a significant role in the generation or even modulation of oscillatory activity at least at relatively low amplitudes of the current.

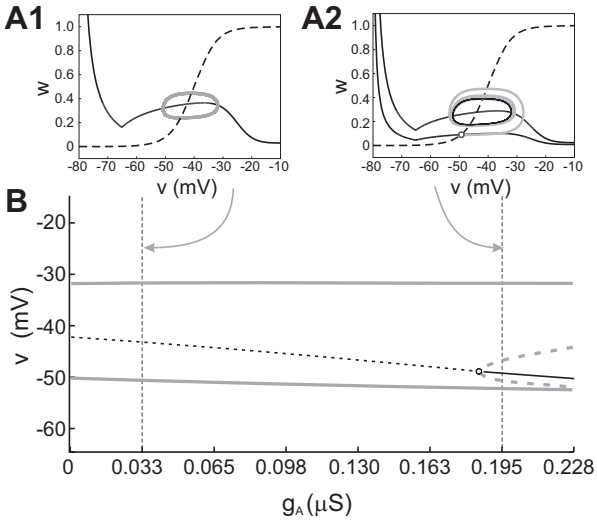

Fig. 9. Effect of I_A on the existence of oscillations. *A1*: projection onto the *v*-*w* phase plane for $g_A = 0.033$ μS. No qualitative difference is found from the $g_A = 0$ μS case (shown in Fig. 8*A1*). The third variable, *h* (not shown), also oscillates but remains small. The *v*-nullcline shown is for the largest value of *h* along the periodic solution. The intersection of the projection of the *v* and *w*-nullclines is not a fixed point. *A2*: projection onto the *v*-*w* phase plane at $g_A = 0.195$ μS for which bistability exists between the periodic solution and a stable fixed point. The lower of the two *v*-nullclines occurs for $h = 0.45$ at the value corresponding to a stable fixed point (open circle). The upper of the 2 *v*-nullclines occurs at the largest *h* value along the periodic solution. *B*: bifurcation diagram showing how the bistability of solutions depends on g_A. Gray curves indicate the voltage limits of oscillatory solutions, whereas the black line indicates a fixed point. Solid and dashed lines, respectively, indicate stable and unstable. Arrows from *A1* and *A2* show the values of g_A used to produce those simulations. The unstable fixed point (dashed black curve) undergoes a subcritical Hopf bifurcation as g_A increases, resulting in a stable fixed point and an unstable branch of periodic solutions.

DISCUSSION

We have shown previously (Zhao et al. 2010) that the nearly linear and negatively sloped portion of the inward modulator-activated current (I_{MI}) is the key element to produce oscillations in pacemaker cells of the pyloric central pattern generator. In crustaceans, the pacemaker of the pyloric network consists of two very strongly electrically coupled cell types, the AB neuron and the PD neurons. The AB neuron is considered to be the primary driver of the pacemaker unit. However, the strong electrical coupling between these cells allows the PD neurons to strongly influence pacemaking activity. In fact, we have shown previously that oscillations can be induced by injecting I_{NL} into either PD or AB neurons (Zhao et al. 2010). In Bose et al. (2014), we addressed the question of what currents are minimally necessary to produce oscillatory activity in a single-cell model of a neural pattern generator. We did so by examining a simplified model of an oscillator consisting of a delayed rectifier K^+ current and a linear inward current that describes the behavior of this negative-conductance component of I_{MI} and which we call the negative-conductance leak current (I_{NL}). That work suggested, but left open, the question of how a balance between inward and distinct outward currents arises in pyloric neurons and whether there are systematic differences in this balance between pacemaker and follower cells. Here, using both experiments and simulations, we provide evidence that pyloric neurons contain different levels of specific outward currents and that this may be the key distinction between what makes a neuron a pacemaker or a follower. In the present study we have focused on the PD neuron of the pacemaker unit. We believe that our conclusion would not be affected if the same were done with the AB neuron, even though some of the quantitative aspects might be affected.

Experimentally, we find that one cell type, the PD neurons, which are considered part of the pacemaker groups of neurons in the network (Marder and Eisen 1984), are the only ones that can generate oscillations when driven by I_{NL}: PD neurons can sustain oscillations over a large but finite range of conductances and equilibrium potentials of I_{NL}. In contrast to the PD neurons, we find that no value of I_{NL} conductance (or combination of g_{NL} and E_{NL}) can induce oscillations in any of the follower neurons. These findings are consistent with the effect of the endogenous neuromodulatory peptide proctolin on the pyloric network neurons (Hooper and Marder 1987; Zhao et al. 2010). Proctolin is one of the neuromodulators that activate I_{MI}, the current for which I_{NL} is a simplified (linear) version. Although proctolin produces oscillations in the pyloric pacemaker neurons, it does not produce oscillations in any of the synaptically isolated pyloric follower neurons (Hooper and Marder 1987; Zhao et al. 2010).

Because pyloric neurons have the same set of ionic currents (Schulz et al. 2006, 2007; Temporal et al. 2012, 2014), we explored the mechanisms that preclude endogenous oscillations in the follower neurons. We found that in follower LP and VD neurons high-threshold outward currents (I_{HTK}) are much too large, compared with the same currents in the PD neuron, to permit I_{NL}-induced oscillations. However, oscillations in both of these follower neuron types could be produced if I_{HTK} was reduced pharmacologically. These results suggest that, to be able to produce endogenous oscillations, a relative balance between the pacemaker current (for which I_{NL} is a surrogate) and the counteracting outward currents needs to be maintained.

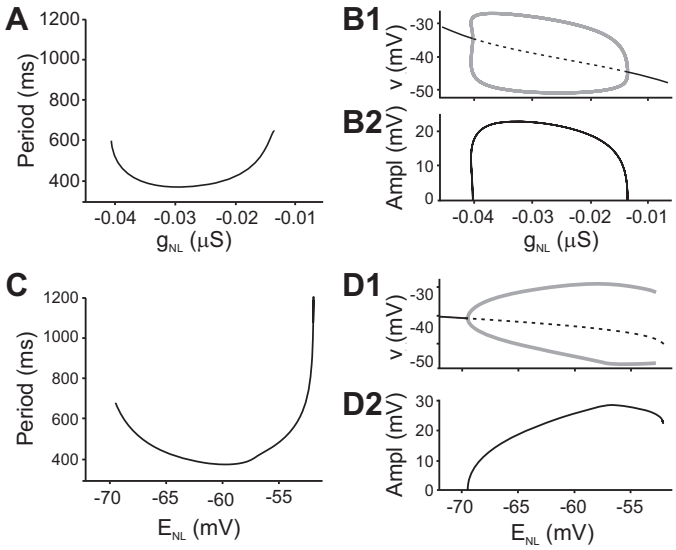

Fig. 10. Effect of I_{NL} parameters on oscillation period and amplitude. *A* and *C* are model analogs of Fig. 2, *B* and *D*, showing how period depends on g_{NL} and E_{NL}, respectively. The simulations qualitatively match the behavior of the experimental system. *B1* and *D1* plot the bifurcation diagrams obtained by respectively varying g_{NL} and E_{NL}. *B2* and *D2* are model analogs of Fig. 2, *C* and *E*, showing how oscillation amplitude depends on g_{NL} and E_{NL}, respectively. Amplitude is calculated as a difference between the minimum (*bottom* gray) and maximum (*top* gray) voltage for each parameter value in *B1* and *D1*. $E_{NL} = -65$ mV in *A* and *B*; $g_{NL} = -0.0195$ μS in *C* and *D*; and $g_A = 0$ μS in all panels.

Interestingly, we also observe that increasing the I_{NL} conductance alone cannot, at least in these cells, balance the high levels of outward currents. To address why the large outward currents cannot simply be balanced by increasing the inward currents, we used a simplified mathematical model. This model confirmed that there is a finite region in the g_{NL}-g_{HTK} space within which oscillations are possible (Fig. 8*E*). The bounds on this region result from either insufficient inward current when g_{HTK} is low (lower edge of oscillation region in Fig. 8*E*) or the inability of I_{NL} to balance the total K^+ currents, which includes two currents, $I_{HTK} + I_{Kdr}$, when I_{HTK} is too high.

Several theoretical studies have suggested that a balance between inward and outward current is required for oscillatory activity to be generated (Doloc-Mihu and Calabrese 2014; Goldman et al. 2001; Hudson and Prinz 2010; Lamb and Calabrese 2013; Zhao and Golowasch 2012). In the leech, it was shown that a close linear correlation between three currents, a leak current, a persistent K^+ current, and a persistent Na^+ current, was required to ensure bursting oscillatory activity (Doloc-Mihu and Calabrese 2014; Lamb and Calabrese 2013). Although in our case the relationship between g_K and g_{NL} is not linear as in the leech studies, but rather bell shaped and broad (Fig. 8*E*), those studies are consistent with ours in that relatively strict relationships must be maintained to ensure the generation of a number of features of activity, including oscillatory and bursting activity. Another example that supports the relationship between oscillatory activity and an inward/outward current balance is that of bursting pacemaker neurons in the rodent pre-Bötzinger respiratory center, in which a higher ratio of persistent Na^+ current to leak current (I_{NaP}/I_{leak}) is characteristic of pacemaker neurons, while a lower ratio is typical of follower neurons (Del Negro et al. 2002).

Studies with cultured STG neurons (Haedo and Golowasch 2006; Turrigiano et al. 1995) have shown that neurons may be programmed to maintain and even restore such relationships after the loss of oscillatory activity. In these studies, recovery of rhythmic activity in cultured crab STG neurons after dissociation required the reduction of I_{HTK} and the increase in inward currents whose voltage dependence resembles that of I_{MI} and I_{NL}. These cells are capable of doing this over the course of hours to days in culture. Thus we conclude that pacemaker activity in individual neurons involves a careful balance, not simply a linear correlation, of an inward pacemaker current with some type of current, such as I_{HTK}, which promotes the recovery from depolarization.

In the STG, I_{HTK} is composed of two high-threshold currents, the delayed rectifier I_{Kdr} and the calcium-dependent I_{KCa}. The former is known to be involved in action potential generation, while I_{KCa} may more directly be involved in oscillatory activity (Haedo and Golowasch 2006; Soto-Treviño et al. 2005). Nevertheless, here [and earlier (Bose et al. 2014)] we showed that I_{Kdr} is also capable of generating oscillatory activity in conjunction with I_{MI} or I_{NL}. In other systems also, high-threshold K^+ currents have been shown to be essential elements of oscillatory mechanisms (e.g., *Aplysia* egg laying; Hermann and Erxleben 1987), but the specific relationship with the inward currents engaged in oscillatory activity in that system has not been examined.

Interestingly, the transient A current does not typically seem to be involved in pacemaker activity generation, as we confirmed in this study, even though its activation properties can be quite similar to those of high-threshold K^+ currents. In our study, I_A has the same voltage dependence of activation as I_{Kdr}, but only I_{Kdr} can participate in the generation of oscillatory activity (see also Bose et al. 2014). Thus the differences in the kinetics and voltage dependencies of the inactivation variable are probably sufficient to determine or exclude its participation in pacemaker activity. Additionally, the transient I_A was not involved in the recovery of rhythmic activity in crab cultured cells (Haedo and Golowasch 2006), consistent with the result reported here.

Our modeling results also provide the basis to interpret and understand some of our experimental results regarding the dependence of period and amplitude on parameters associated with I_{NL}. They show that in most cases the results are qualitatively consistent over a subset of parameter values of the model. A comparison between Fig. 2, *B–E* (experimental results) and Fig. 10 (model results) relative to how period and amplitude vary with g_{NL} and E_{NL}, for example, reveals a consistent relative independence of cycle period on g_{NL} (Fig. 2*B*). In the model, changes in g_{NL} simply shifted the *v*-nullcline up or down in the phase space but left the overall balance of currents largely intact over a large range of values. As a result, neither period nor amplitude varies much (Fig. 10, *A* and *B*). Variations due to changes in E_{NL} were also consistent across both experiment and model. When E_{NL} becomes too small, the inward effect of I_{NL} is mitigated by the outward effect of I_{Kdr} (their reversal potentials are too close). Alternatively, when E_{NL} is too large the model cell is attracted to a higher-level stable fixed point because the inward effect is too strong to be overcome (the driving force from I_{NL} is too large). The model also makes predictions about how oscillations are lost through specific kinds of bifurcations as g_{NL} or E_{NL} are varied. It would be of interest to test whether these predictions are borne out experimentally, which would provide further insight into the mechanisms of rhythm generation in pacemaker neurons similar to pyloric pacemaker neurons.

In conclusion, we observe that a coordinated balance of high-threshold outward currents and inward pacemaker currents is required for the generation of oscillatory activity. This is consistent with previous experimental and theoretical observations, but here we show both approaches confirming this in the same biological system and using a minimal model that captures the essential features of these relationships.

ACKNOWLEDGMENTS

Preprint available at https://doi.org/10.1101/136887.

GRANTS

This work was supported by National Science Foundation Grant DMS1122291 (A. Bose), National Institutes of Health (NIH) Grants MH-064711 and NS-085330 (J. Golowasch), and NIH Grant MH-060605 (F. Nadim).

DISCLOSURES

No conflicts of interest, financial or otherwise, are declared by the authors.

AUTHOR CONTRIBUTIONS

J.G., A.B., and F.N. conceived and designed research; J.G., A.B., Y.G., D.S., and F.N. analyzed data; J.G., A.B., and F.N. interpreted results of

experiments; J.G., A.B., and F.N. prepared figures; J.G., A.B., and F.N. drafted manuscript; J.G., A.B., and F.N. edited and revised manuscript; J.G., A.B., Y.G., D.S., A.R., and F.N. approved final version of manuscript; A.B., Y.G., D.S., and A.R. performed experiments.

REFERENCES

Amarillo Y, Zagha E, Mato G, Rudy B, Nadal MS. The interplay of seven subthreshold conductances controls the resting membrane potential and the oscillatory behavior of thalamocortical neurons. *J Neurophysiol* 112: 393–410, 2014. doi:10.1152/jn.00647.2013.

Amendola J, Woodhouse A, Martin-Eauclaire MF, Goaillard JM. Ca^{2+}/cAMP-sensitive covariation of I_A and I_H voltage dependences tunes rebound firing in dopaminergic neurons. *J Neurosci* 32: 2166–2181, 2012. doi:10.1523/JNEUROSCI.5297-11.2012.

Anderson WD, Makadia HK, Vadigepalli R. Molecular variability elicits a tunable switch with discrete neuromodulatory response phenotypes. *J Comput Neurosci* 40: 65–82, 2016. doi:10.1007/s10827-015-0584-2.

Anirudhan A, Narayanan R. Analogous synaptic plasticity profiles emerge from disparate channel combinations. *J Neurosci* 35: 4691–4705, 2015. doi:10.1523/JNEUROSCI.4223-14.2015.

Bayliss DA, Viana F, Berger AJ. Mechanisms underlying excitatory effects of thyrotropin-releasing hormone on rat hypoglossal motoneurons in vitro. *J Neurophysiol* 68: 1733–1745, 1992.

Bergquist S, Dickman DK, Davis GW. A hierarchy of cell intrinsic and target-derived homeostatic signaling. *Neuron* 66: 220–234, 2010. doi:10.1016/j.neuron.2010.03.023.

Blethyn KL, Hughes SW, Tóth TI, Cope DW, Crunelli V. Neuronal basis of the slow (<1 Hz) oscillation in neurons of the nucleus reticularis thalami in vitro. *J Neurosci* 26: 2474–2486, 2006. doi:10.1523/JNEUROSCI.3607-05.2006.

Bose A, Golowasch J, Guan Y, Nadim F. The role of linear and voltage-dependent ionic currents in the generation of slow wave oscillations. *J Comput Neurosci* 37: 229–242, 2014. doi:10.1007/s10827-014-0498-4.

Brickley SG, Aller MI, Sandu C, Veale EL, Alder FG, Sambi H, Mathie A, Wisden W. TASK-3 two-pore domain potassium channels enable sustained high-frequency firing in cerebellar granule neurons. *J Neurosci* 27: 9329–9340, 2007. doi:10.1523/JNEUROSCI.1427-07.2007.

Cymbalyuk GS, Gaudry Q, Masino MA, Calabrese RL. Bursting in leech heart interneurons: cell-autonomous and network-based mechanisms. *J Neurosci* 22: 10580–10592, 2002.

Del Negro CA, Koshiya N, Butera RJ Jr, Smith JC. Persistent sodium current, membrane properties and bursting behavior of pre-bötzinger complex inspiratory neurons in vitro. *J Neurophysiol* 88: 2242–2250, 2002. doi:10.1152/jn.00081.2002.

Doloc-Mihu A, Calabrese RL. Identifying crucial parameter correlations maintaining bursting activity. *PLOS Comput Biol* 10: e1003678, 2014. doi:10.1371/journal.pcbi.1003678.

Dunmyre JR, Del Negro CA, Rubin JE. Interactions of persistent sodium and calcium-activated nonspecific cationic currents yield dynamically distinct bursting regimes in a model of respiratory neurons. *J Comput Neurosci* 31: 305–328, 2011. doi:10.1007/s10827-010-0311-y.

Egorov AV, Hamam BN, Fransén E, Hasselmo ME, Alonso AA. Graded persistent activity in entorhinal cortex neurons. *Nature* 420: 173–178, 2002. doi:10.1038/nature01171.

Ermentrout B. *Simulating, Analyzing, and Animating Dynamical Systems: a Guide to XPPAUT for Researchers and Students*. Philadelphia, PA: Society for Industrial and Applied Mathematics, 2002, p. xiv. doi:10.1137/1.9780898718195.

Goaillard JM, Taylor AL, Schulz DJ, Marder E. Functional consequences of animal-to-animal variation in circuit parameters. *Nat Neurosci* 12: 1424–1430, 2009. doi:10.1038/nn.2404.

Goldman MS, Golowasch J, Marder E, Abbott LF. Global structure, robustness, and modulation of neuronal models. *J Neurosci* 21: 5229–5238, 2001.

Golowasch J. Stability and homeostasis in small network central pattern generators. In: *Encyclopedia of Computational Neuroscience*, edited by Jaeger D, Jung R. New York: Springer, 2015, p. 2858–2864. doi:10.1007/978-1-4614-6675-8_466.

Golowasch J, Marder E. Ionic currents of the lateral pyloric neuron of the stomatogastric ganglion of the crab. *J Neurophysiol* 67: 318–331, 1992a.

Golowasch J, Marder E. Proctolin activates an inward current whose voltage dependence is modified by extracellular Ca^{2+}. *J Neurosci* 12: 810–817, 1992b.

Gray M, Golowasch J. Voltage dependence of a neuromodulator-activated ionic current. *eNeuro* 3: 22, 2016. doi:10.1523/ENEURO.0038-16.2016.

Haedo RJ, Golowasch J. Ionic mechanism underlying recovery of rhythmic activity in adult isolated neurons. *J Neurophysiol* 96: 1860–1876, 2006. doi:10.1152/jn.00385.2006.

Hermann A, Erxleben C. Charybdotoxin selectively blocks small Ca-activated K channels in *Aplysia* neurons. *J Gen Physiol* 90: 27–47, 1987. doi:10.1085/jgp.90.1.27.

Hooper SL, Marder E. Modulation of the lobster pyloric rhythm by the peptide proctolin. *J Neurosci* 7: 2097–2112, 1987.

Hudson AE, Prinz AA. Conductance ratios and cellular identity. *PLOS Comput Biol* 6: e1000838, 2010. doi:10.1371/journal.pcbi.1000838.

Jahnsen H, Llinás R. Ionic basis for the electro-responsiveness and oscillatory properties of guinea-pig thalamic neurones in vitro. *J Physiol* 349: 227–247, 1984. doi:10.1113/jphysiol.1984.sp015154.

Khorkova O, Golowasch J. Neuromodulators, not activity, control coordinated expression of ionic currents. *J Neurosci* 27: 8709–8718, 2007. doi:10.1523/JNEUROSCI.1274-07.2007.

Koizumi H, Smith JC. Persistent Na^+ and K^+-dominated leak currents contribute to respiratory rhythm generation in the pre-Bötzinger complex in vitro. *J Neurosci* 28: 1773–1785, 2008. doi:10.1523/JNEUROSCI.3916-07.2008.

Lamb DG, Calabrese RL. Correlated conductance parameters in leech heart motor neurons contribute to motor pattern formation. *PLoS One* 8: e79267, 2013. doi:10.1371/journal.pone.0079267.

Linsdell P, Moody WJ. Na^+ channel mis-expression accelerates K^+ channel development in embryonic *Xenopus laevis* skeletal muscle. *J Physiol* 480: 405–410, 1994. doi:10.1113/jphysiol.1994.sp020370.

Lu TZ, Feng ZP. NALCN: a regulator of pacemaker activity. *Mol Neurobiol* 45: 415–423, 2012. doi:10.1007/s12035-012-8260-2.

Lutas A, Lahmann C, Soumillon M, Yellen G. The leak channel NALCN controls tonic firing and glycolytic sensitivity of substantia nigra pars reticulata neurons. *eLife* 5: e15271, 2016. doi:10.7554/eLife.15271.

MacLean JN, Zhang Y, Johnson BR, Harris-Warrick RM. Activity-independent homeostasis in rhythmically active neurons. *Neuron* 37: 109–120, 2003. doi:10.1016/S0896-6273(02)01104-2.

Marder E, Eisen JS. Electrically coupled pacemaker neurons respond differently to same physiological inputs and neurotransmitters. *J Neurophysiol* 51: 1362–1374, 1984.

McCormick DA, Huguenard JR. A model of the electrophysiological properties of thalamocortical relay neurons. *J Neurophysiol* 68: 1384–1400, 1992.

Pang DS, Robledo CJ, Carr DR, Gent TC, Vyssotski AL, Caley A, Zecharia AY, Wisden W, Brickley SG, Franks NP. An unexpected role for TASK-3 potassium channels in network oscillations with implications for sleep mechanisms and anesthetic action. *Proc Natl Acad Sci USA* 106: 17546–17551, 2009. doi:10.1073/pnas.0907228106.

Rekling JC, Funk GD, Bayliss DA, Dong XW, Feldman JL. Synaptic control of motoneuronal excitability. *Physiol Rev* 80: 767–852, 2000.

Roffman RC, Norris BJ, Calabrese RL. Animal-to-animal variability of connection strength in the leech heartbeat central pattern generator. *J Neurophysiol* 107: 1681–1693, 2012. doi:10.1152/jn.00903.2011.

Schulz DJ, Goaillard JM, Marder E. Variable channel expression in identified single and electrically coupled neurons in different animals. *Nat Neurosci* 9: 356–362, 2006. doi:10.1038/nn1639.

Schulz DJ, Goaillard JM, Marder EE. Quantitative expression profiling of identified neurons reveals cell-specific constraints on highly variable levels of gene expression. *Proc Natl Acad Sci USA* 104: 13187–13191, 2007. doi:10.1073/pnas.0705827104.

Selverston AI, Russell DF, Miller JP, King DG. The stomatogastric nervous system: structure and function of a small neural network. *Prog Neurobiol* 7: 215–290, 1976. doi:10.1016/0301-0082(76)90008-3.

Soto-Treviño C, Rabbah P, Marder E, Nadim F. Computational model of electrically coupled, intrinsically distinct pacemaker neurons. *J Neurophysiol* 94: 590–604, 2005. doi:10.1152/jn.00013.2005.

Srikanth S, Narayanan R. Variability in state-dependent plasticity of intrinsic properties during cell-autonomous self-regulation of calcium homeostasis in hippocampal model neurons. *eNeuro* 2: ENEURO.0053-15.2015, 2015. doi:10.1523/ENEURO.0053-15.2015.

Swensen AM, Marder E. Multiple peptides converge to activate the same voltage-dependent current in a central pattern-generating circuit. *J Neurosci* 20: 6752–6759, 2000.

Talley EM, Lei Q, Sirois JE, Bayliss DA. TASK-1, a two-pore domain K^+ channel, is modulated by multiple neurotransmitters in motoneurons. *Neuron* 25: 399–410, 2000. doi:10.1016/S0896-6273(00)80903-4.

Temporal S, Desai M, Khorkova O, Varghese G, Dai A, Schulz DJ, Golowasch J. Neuromodulation independently determines correlated channel expression and conductance levels in motor neurons of the stomatogastric ganglion. *J Neurophysiol* 107: 718–727, 2012. doi:10.1152/jn.00622.2011.

Temporal S, Lett KM, Schulz DJ. Activity-dependent feedback regulates correlated ion channel mRNA levels in single identified motor neurons. *Curr Biol* 24: 1899–1904, 2014. doi:10.1016/j.cub.2014.06.067.

Turrigiano G, LeMasson G, Marder E. Selective regulation of current densities underlies spontaneous changes in the activity of cultured neurons. *J Neurosci* 15: 3640–3652, 1995.

van den Top M, Lee K, Whyment AD, Blanks AM, Spanswick D. Orexigen-sensitive NPY/AgRP pacemaker neurons in the hypothalamic arcuate nucleus. *Nat Neurosci* 7: 493–494, 2004. doi:10.1038/nn1226.

Vandermaelen CP, Aghajanian GK. Electrophysiological and pharmacological characterization of serotonergic dorsal raphe neurons recorded extracellularly and intracellularly in rat brain slices. *Brain Res* 289: 109–119, 1983. doi:10.1016/0006-8993(83)90011-2.

Xu XF, Tsai HJ, Li L, Chen YF, Zhang C, Wang GF. Modulation of leak K^+ channel in hypoglossal motoneurons of rats by serotonin and/or variation of pH value. *Sheng Li Xue Bao* 61: 305–316, 2009.

Yamada-Hanff J, Bean BP. Persistent sodium current drives conditional pacemaking in CA1 pyramidal neurons under muscarinic stimulation. *J Neurosci* 33: 15011–15021, 2013. doi:10.1523/JNEUROSCI.0577-13.2013.

Zhao S, Golowasch J. Ionic current correlations underlie the global tuning of large numbers of neuronal activity attributes. *J Neurosci* 32: 13380–13388, 2012. doi:10.1523/JNEUROSCI.6500-11.2012.

Zhao S, Golowasch J, Nadim F. Pacemaker neuron and network oscillations depend on a neuromodulator-regulated linear current. *Front Behav Neurosci* 4: 21, 2010.